https://doi.org/10.5194/egusphere-2025-3914
Preprint. Discussion started: 2 September 2025

A Comparative Analysis of China's Anthropogenic CO_2 Emissions (2000–2023): Insights from Six Bottom-Up Inventories and Uncertainty Assessment

Huirong Yang[1,2,3], Kai Wu[1,3], Huizhong Shen[4,5], Greet Janssens-Maenhout[6], Monica Crippa[6], Diego Guizzardi[6], Minqiang Zhou[1,3]

[1]Key Laboratory of Atmospheric Environment and Extreme Meteorology, Institute of Atmospheric Physics, Chinese Academy of Sciences, Beijing, 100029, China
[2]University of Chinese Academy of Sciences, Beijing, 101408, China
[3]LAGEO & CNRC, Institute of Atmospheric Physics, Chinese Academy of Sciences, Beijing, 100029, China
[4]Guangdong Provincial Observation and Research Station for Coastal Atmosphere and Climate of the Greater Bay Area, School of Environmental Science and Engineering, Southern University of Science and Technology, Shenzhen, 518055, China
[5]Shenzhen Key Laboratory of Precision Measurement and Early Warning Technology for Urban Environmental Health Risks, School of Environmental Science and Engineering, Southern University of Science and Technology, Shenzhen, 518055, China
[6] European Commission, Joint Research Centre (JRC), Ispra (VA), 21027, Italy

Correspondence to: Kai Wu (kwu@mail.iap.ac.cn) and Minqiang Zhou (minqiang.zhou@mail.iap.ac.cn)

Abstract. Accurate quantification of anthropogenic CO_2 emissions is crucial for mitigating climate change and verifying emission reduction policies. This study conducts a comparative analysis of China's anthropogenic CO_2 emissions for the period between 2000 and 2023 based on six widely used bottom-up inventories at their latest version (ODIAC2023, EDGAR2024, MEIC-global-CO_2 v1.0, CAMS-GLOB-ANT v6.2, GEMS v1.0, and CEADs). The national total CO_2 emissions increase from 3.43 (3.21–3.63) Gt year^{-1} in 2000 to 12.03 (11.35–12.98) Gt year^{-1} in 2023, with three growth periods: rapid growth (2000–2012, 0.56±0.015 Gt year^{-1}), near-stagnation (2012–2016, 0.01±0.045 Gt year^{-1}), and renewed growth (2016–2023, 0.30±0.016 Gt year^{-1}). Emissions are dominated by the electricity and heat production, and the industry and construction (78% of total emissions), with the former replacing the latter as the largest source after 2017. EDGAR consistently reports the highest national CO_2 emissions, while MEIC provides the lowest, contributing to the large deviations after 2012. EDGAR and MEIC report different spatial distributions of the transport sector. EDGAR concentrates emissions along major roads and MEIC distributes them more diffusely. Extreme outliers (>10^5 ton CO_2 km^{-2} year^{-1}, against an average of 10^2 ton CO_2 km^{-2} year^{-1}) in these inventories arise from discrepancies in point source data in the Carbon Monitoring for Action (CARMA) versus the China Power Emissions Database (CPED). Overall, the uncertainty of total national anthropogenic CO_2 emissions is within 5% (1σ), and the uncertainties are about 10–50% (1σ) at the provincial level.

https://doi.org/10.5194/egusphere-2025-3914
Preprint. Discussion started: 2 September 2025

1 Introduction

The global mean temperature in 2024 was 1.5°C above pre-industrial levels, making it the warmest year in the 175-year record of observations (WMO, 2025). This increases the urgency of achieving the Paris Agreement's goal of limiting global warming to a maximum of 1.5°C (Schleussner et al., 2016). Atmospheric carbon dioxide (CO_2) is the dominant greenhouse gas (IPCC, 2017), and its concentration (430.5 ppm in May 2025) is now 1.5 times higher than pre-industrial levels (280 ppm), mainly due to anthropogenic activities (WMO 2024; Etheridge et al., 1996). China, which is responsible for about 80% of East Asia's anthropogenic CO_2 emissions (Xia et al., 2025), has committed to reaching peak emissions by 2030 and carbon neutrality by 2060. To achieve these targets, accurate quantification of anthropogenic CO_2 emissions and understanding the uncertainties in emissions inventories are needed to guide emission reduction policies (Li et al., 2017a).

A variety of bottom-up emission inventories have been developed to quantify anthropogenic CO_2 emissions based on activity data and emission factors (EFs). The gridded inventories apply spatial proxies to allocate emissions across grid cells (Han et al., 2020a), including point sources (e.g., power plants), line sources (e.g., road networks), and area sources (e.g., population density, gross domestic product (GDP), nighttime lights). Global gridded products provide consistent, worldwide estimates with high spatial resolution (1 km or 0.1°), such as the Open-Data Inventory for Anthropogenic Carbon Dioxide (ODIAC) (Oda et al., 2018; Oda and Maksyutov, 2011), the Emissions Database for Global Atmospheric Research (EDGAR) (Janssens-Maenhout et al., 2019), and the Global Emission Modeling System (GEMS) (Wang et al., 2013). China-specific inventories use provincial energy statistics and locally optimized EFs to account for national and subnational CO_2 emissions, such as the Multi-resolution Emission Inventory for China (MEIC) (R. Xu et al., 2024; Li et al., 2017a; B. Zheng et al., 2018), the China High Resolution Emission Database (CHRED) (Cai et al., 2018) and the China Emission Accounts and Datasets (CEADs) (J. Xu et al., 2024; Y. Guan et al., 2021; Shan et al., 2018, 2020).

Despite the different allocation methods and underlying data, the uncertainties in the overall magnitudes and trends of CO_2 emissions between the global inventories are within 10% at the global scale (Oda et al., 2019; Han et al., 2020a; R. Xu et al., 2024). However, at the national scale, the uncertainties can reach 40-100% (Peylin et al., 2013) and can be even larger at the regional and city scales, e.g., 300% in the Beijing-Tianjin-Hebei area (Han et al., 2020b). The uncertainties between the different inventories are caused by three factors. First, different official statistics can lead to large emission gaps (D. Guan et al., 2012; Hong et al., 2017). Previous studies have shown significant discrepancies in energy consumption from different official statistics in China. Provincial-level data tend to align more closely with satellite observations than national-level statistics (Akimoto et al., 2006; D. Guan et al., 2012; Zhao et al., 2012). Second, the EF is another key element that causes the differences. The IPCC-based EFs used by ODIAC and EDGAR may not correctly reflect the specific fuel quality and combustion technologies in China (e.g., the EF for raw coal in CEADs and ODIAC is 0.499 and 0.746, respectively) (Han et al., 2020a). Third, spatial proxies determine how emissions are distributed across grid cells. For example, relying on outdated point-source databases such as the Carbon Monitoring for Action (CARMA) (the last update was on 28 November, 2012) may incorrectly distribute emissions in urban areas and introduce extrapolation errors (Han et al., 2020a; Wang et al., 2013; M. Liu

https://doi.org/10.5194/egusphere-2025-3914
Preprint. Discussion started: 2 September 2025

et al., 2013), while more comprehensive power plant inventories such as the China Power Emissions Database (CPED) provide better spatial accuracy (Li et al., 2017b; F. Liu et al., 2015).

Previous studies have demonstrated large discrepancies among anthropogenic CO_2 emission inventories in China and investigated the possible reasons. Han et al (2020a) compared nine global and regional inventories for China and found that differences in activity data and EFs can lead to significant uncertainties in emission estimates, with the maximum difference in 2012 reaching up to 33.8%. L. Zheng et al (2025) conducted a cross-scale comparison of EDGAR, MEIC, and CEADs and showed that coarse aggregation reduces the impact of outlier emission values, and leads to stronger agreement between inventories at a resolution of $3° \times 3°$ compared to $0.25° \times 0.25°$. At the city level, Liu et al (2024) found that the relative standard deviations between six inventories are more than 50%, with uncertainties showing a strong logarithmic dependence on proxy variables such as population density and nightlight data. In recent years, China has announced a series of policy measures aimed at reducing carbon emissions, alongside changes in factory technology and energy structure. These developments underscore the urgent need for accurate and timely quantification of anthropogenic CO_2 emissions. Moreover, emission inventories are continuously updated to incorporate improved inputs (e.g., activity data, EFs, and refined methodology). Therefore, it is crucial to use the latest versions of the various inventories to better understand the recent changes in China's anthropogenic CO_2 emissions.

To this aim, this study conducts a comprehensive analysis of the spatiotemporal variation of China's anthropogenic CO_2 emissions and investigates the differences among six widely used emission inventories at their latest versions: the global inventories ODIAC, EDGAR, MEIC, GEMS, and the global anthropogenic emissions for the Copernicus Atmosphere Monitoring Service (CAMS-GLOB-ANT, hereafter referred to as CAMS), and the China-specific inventory CEADs. The data and methods are presented in Section 2. We report our results in Section 3 and conclude the paper in Section 4.

2 Data and methods

Six anthropogenic CO_2 emission inventories, including five gridded inventories (ODIAC2023, EDGAR2024, MEIC-global-CO_2 v1.0, CAMS v6.2, and GEMS v1.0) and one urban total emission inventory (CEADs), are applied to provide estimates of total emissions at the national, provincial, and city levels in China. The specific information of these inventories is presented in Section 2.1. Table 1 lists the temporal and spatial resolution, data version, and principal downscaling proxies of those inventories. All five gridded inventories were standardized to a common $0.1° \times 0.1°$ coordinate system and a common unit of ton CO_2 km^{-2} year^{-1} (Section 2.2).

https://doi.org/10.5194/egusphere-2025-3914
Preprint. Discussion started: 2 September 2025

Table 1. Specification of emission inventory statistics.

	ODIAC	EDGAR	MEIC	CAMS	GEMS	CEADs
Version	ODIAC2023	EDGAR2024	v1.0	v6.2	v1.0	NA
Domain	Global	Global	Global	Global	Global	China
Temporal coverage	2000-2022	1970-2023	1970-2023	2000-2026	1700-2019	1997-2021
Time resolution	Monthly or annual	Monthly or annual	Monthly or annual	Monthly or annual	Monthly or annually	Annual
Point source	CARMA	CARMA	CPED	EDGAR	WRI	NA
Line source	NA	OpenStreetMap and OpenRailwayMap	CDRM	EDGAR	NA	NA
Area source	Nightlight data	Population density and nightlight data	Population density and land use	Population density	Population density, nightlight data and vegetation density	NA
Spatial resolution	1km×1km, 1°×1°	0.1°×0.1°	0.1°×0.1°	0.1°×0.1°	0.1°×0.1°	NA
Unit of gridded emissions	ton C cell^{-1} month^{-1}	ton CO_2 km^{-2} year^{-1}	ton CO_2 cell^{-1} year^{-1}	kg CO_2 m^{-2} s^{-1}	g CO_2 km^{-2} year^{-1}	NA
Emission estimates	Global	Global and national	Global, national and provincial	Global and National	Global and national	National, provincial and city
Year published	2024	2024	2024	2023	2024	2017
Data source	https://db.cger.nies.go.jp/dataset/ODIAC/DL_odiac	https://edgar.jrc.ec.europa.eu/dataset_ghg2	http://meicmodel.org.cn/?page_id=2341	https://eccad.sedoo.fr/#/metadata/	https://gems.pku.edu.cn/data/database	https://www.ceads.net.cn/data/

https://doi.org/10.5194/egusphere-2025-3914
Preprint. Discussion started: 2 September 2025

	2023.html (last access: 19 April 2025)	024#p1 (last access: 19 April 2025)	(last access: 19 April 2025)	479 (last access: 19 April 2025)	(last access: 19 April 2025)	(last access: 19 April 2025)
References	Oda and Maksyutov (2011); Oda et al (2018)	Janssens-Maenhout et al (2019)	R. Xu et al (2024)	Soulie et al (2024);	Wang et al (2013)	J. Xu et al (2024); Y. Guan et al (2021b); Shan et al (2020, 2018)

2.1 Emission inventories

ODIAC is a global grid-based CO_2 inventory that provides monthly emissions at a high spatial resolution of 1 km × 1 km. Total emissions are derived from the Carbon Dioxide Information Analysis Center (CDIAC), which compiles CO_2 estimates from fossil fuel combustion, cement production, and gas flaring using United Nations energy statistics (Andres et al., 2016; Oda et al., 2018, 2019). These national totals are then spatially allocated for point sources using the CARMA power plant database and for area sources using satellite-based nightlight data. ODIAC does not explicitly map line sources such as road traffic. Although streetlights have been proposed as a proxy for such sources (Oda and Maksyutov, 2011), this approach may over-allocate emissions in brightly lit urban areas relative to rural or low-light regions due to the complexity of actual traffic distribution (Wang et al., 2013). We use ODIAC2023, which covers the years from 2000 to 2022.

EDGAR is developed by the Joint Research Centre (JRC) and the Netherlands Environmental Assessment Agency. It combines national energy balance data from the International Energy Agency (IEA) with sector-specific activity data from sources such as BP plc, the United States Geological Survey (USGS), the World Steel Association, the Global Gas Flaring Reduction Partnership (GGFR), the National Oceanic and Atmospheric Administration (NOAA), and the International Fertilizer Association (IFA). Emissions are calculated using IPCC default EFs and spatially disaggregated using CARMA (point source), OpenStreetMap (line source), and population density and nighttime lights (area sources). We use EDGAR2024, which provides annual and monthly data from 1970 to 2023 at a spatial resolution of 0.1° × 0.1°.

MEIC is developed by Tsinghua University to estimate global and regional CO_2 emissions, with a particular focus on China. Emissions are estimated by integrating activity data from multiple international and local statistics, with 72% of global CO_2 emissions estimated based on information from individual countries in 2021. In China, the energy statistics data is obtained from the provincial-level database: China Energy Statistics Yearbook (CESY). Point emissions are allocated using the China coal-fired Power plant Emissions Database (CPED), which includes more than 7600 generating units—approximately 1300 additional small power plants more than CARMA—and has been validated using satellite imagery. MEIC uses the transportation network data from the China Digital Road Network Map (CDRM) to constrain the distribution of vehicle activity as well as population density, GDP, and land use for other sectors (Li et al., 2017a; Xu et al., 2024b). We use the MEIC-global-

https://doi.org/10.5194/egusphere-2025-3914
Preprint. Discussion started: 2 September 2025

CO_2 product v1.0, the latest version with a spatial resolution of 0.1°, covering the period from 1970 to 2023 at monthly and annual resolutions.

CAMS is a global inventory developed as part of the Copernicus Atmosphere Monitoring Service project. It builds on EDGAR and integrates several complementary datasets, including the Community Emissions Data System (CEDS), the CAMS-GLOB-TEMPO for temporal emission profiles, and the CAMS-GLOB-SHIP for ship emissions. CAMS provides monthly emissions of 36 compounds (GHGs and major air pollutants) across 17 emission sectors (e.g., transportation, electricity generation, industry, etc.) at a resolution of 0.1° × 0.1° (Soulie et al., 2024). The version used in this study is CAMS-GLOB-ANT v6.2, which covers the period from 2000 to 2026.

GEMS is a global CO_2 inventory that is developed as a successor to Peking University CO_2 (PKU). It updates the EFs based on the latest literature and on-site measurements, and refines the technology splits in sectors such as road transport. The energy statistics come from the National Bureau of Statistics (NBS) for China and from sub-national datasets for many developed and developing countries. For countries lacking sub-national fuel consumption data, national-level statistics from IEA are used. Emissions are classified into seven sectors (power generation, industry, residential and commercial emissions, transportation, agriculture, and natural emissions) or six fuel/activity types (coal, oil, gas, waste, biomass, and industrial processes). The spatial allocation uses World Resources Institute (WRI) for point sources and combines vegetation density, population density, and nighttime lights for the remaining emissions (Wang et al., 2013). We use GEMS v1.0, which covers the period 1700–2021 with a spatial resolution of 0.1°. However, the version available at the time of our analysis only included data up to 2019, which is therefore the endpoint used throughout our study.

CEADs provides annual CO_2 emissions at national, provincial, and city scales. The national and provincial emissions are based on CESY and NBS, respectively. In addition to total CO_2 emissions, CEADs provides an energy inventory, a CO_2 emission inventory for industrial processes, and EFs. CEADs uses locally optimized EFs derived from extensive sample measurements—such as 602 coal samples and over 4000 coal mines for coal EFs—which are considered more representative of China's actual fuel characteristics than the IPCC-based default values (Shan et al., 2018, 2020; J. Xu et al., 2024; Y. Guan et al., 2021). In this study, we use the national and provincial CEADs datasets from 2000 to 2021.

2.2 Data preprocessing

To extract the data, we first used a mask with national boundaries (https://cloudcenter.tianditu.gov.cn/administrativeDivision) to extract the emissions within mainland China for the five global grid-based inventories (ODIAC, EDGAR, MEIC, CAMS, and GEMS). To enable consistent comparison between inventories, all gridded datasets were processed to a uniform spatial resolution of 0.1° × 0.1°, with emission units standardized to ton CO_2 km^{-2} year^{-1}. Unit conversions accounted for original formats and required area normalization for datasets with grid-cell-based values (e.g., ODIAC: ton C cell^{-1} month^{-1}, MEIC: ton CO_2 cell^{-1} year^{-1}). A stoichiometric factor (44/12) was applied to convert carbon to CO_2 where necessary (e.g., ODIAC). Spatial resampling was performed to align with the MEIC coordinate system, using nearest-neighbor interpolation or area-weighted aggregation depending on the original resolution. National totals were taken directly from original reports, except

https://doi.org/10.5194/egusphere-2025-3914
Preprint. Discussion started: 2 September 2025

for ODIAC, which was summed from gridded data. At the provincial level, emissions were taken directly from the MEIC and CEADs data, while for the other datasets, estimates for the provinces were calculated using spatial zonal statistics based on standardized administrative boundary masks (https://cloudcenter.tianditu.gov.cn/administrativeDivision).

3 Results

3.1 National total CO_2 emissions

The six bottom-up inventories show a significant increase in total national CO_2 emissions from 2000 to 2023 (GEMS to 2019, CEADs to 2021, ODIAC to 2022), with average emissions increasing from 3.43 Gt year^{-1} in 2000 to 12.03 Gt year^{-1} in 2023 (Fig. 1). The differences between the emission inventories become more pronounced after 2012 and diverge in recent years, with the emission range (maximum-minimum difference) and the standard deviation (SD) increasing from 0.41 and 0.14 Gt year^{-1} in 2000 to 1.63 and 0.58 Gt year^{-1} in 2023. Before 2012, both metrics are relatively stable and low (range < 0.82 Gt year^{-1}, SD < 0.30 Gt year^{-1}). After 2013, however, the range is above 1.03 Gt year^{-1} and peaked at 1.64 Gt year^{-1} in 2021, mainly due to EDGAR reporting the highest emissions versus MEIC reporting the lowest emissions.

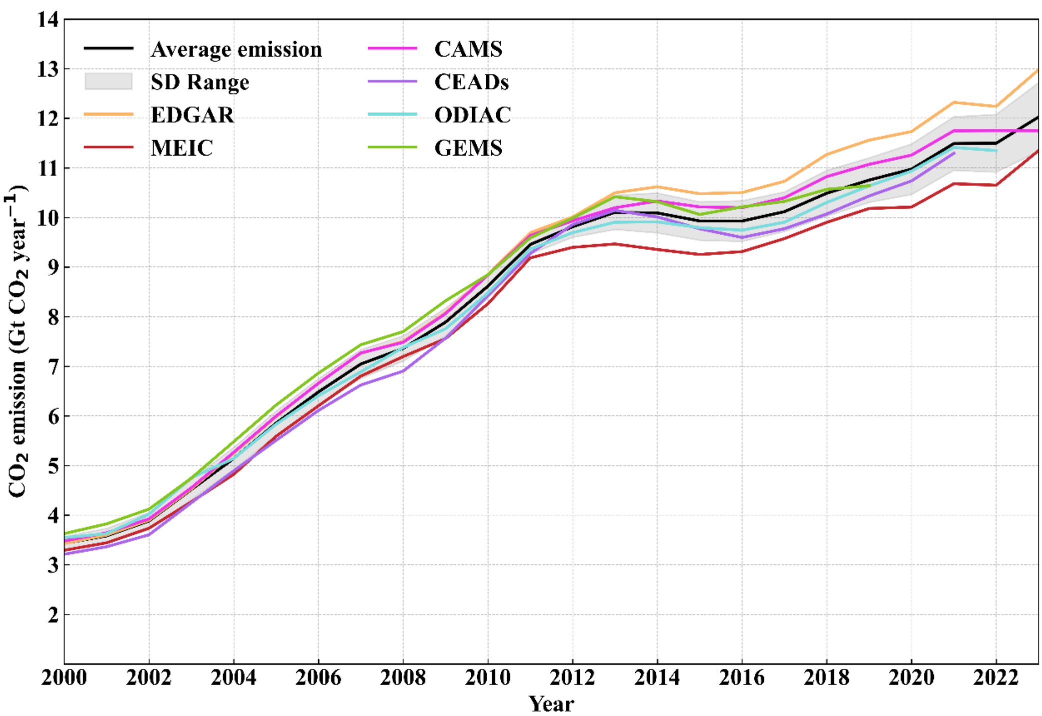

Figure 1. Annual anthropogenic CO_2 emissions in mainland China from 2000 to 2023, as reported by six emission inventories: EDGAR, MEIC, CAMS, CEADs (up to 2021), ODIAC (up to 2022), and GEMS (up to 2019). Apart from ODIAC, all inventories provide national totals directly. We calculated China's emissions by summing the grid values within China for ODIAC. The shaded area indicates the standard deviation of the six inventories.

https://doi.org/10.5194/egusphere-2025-3914
Preprint. Discussion started: 2 September 2025

The increase in CO_2 emissions shows three different phases (Fig. 1, Table 2). The first phase (2000–2012) shows the most rapid growth, with an average growth rate of 0.56 ± 0.015 Gt year^{-1}, driven by industrialization, urbanization, and rising energy demand. In contrast, emissions become relatively stable from 2012 to 2016 under the influence of adjustment of energy structure and industrial upgrades implemented as part of China's 12th Five-Year Plan (Han 2020a; L. Zheng et al., 2025), resulting in an average annual increase rate of 0.01 ± 0.045 Gt year^{-1} and slightly negative rates in MEIC (-0.04 ± 0.02 Gt year^{-1}), CEADs (-0.09 ± 0.057 Gt year^{-1}), and ODIAC (-0.001 ± 0.035 Gt year^{-1}). From 2016 to 2023, all inventories show increased CO_2 emissions again, with a slower rate (0.30 ± 0.016 Gt year^{-1}) compared to the first phase.

Table 2. Linear regression statistics (correlation coefficient (R) and slope with its uncertainty) between CO_2 emissions and year for all six inventories and their average.

		Average emissions	EDGAR	MEIC	CAMS	CEADs	ODIAC	GEMS
2000-2012	Slope	0.56	0.58	0.55	0.57	0.57	0.54	0.56
	Uncertainty of slope	0.015	0.016	0.016	0.016	0.019	0.014	0.014
	R	0.99***	0.99***	0.99***	0.99***	0.99***	0.99***	0.99***
2012-2016	Slope	0.01	0.10	-0.04	0.05	-0.09	-0.00	0.09
	Uncertainty of slope	0.045	0.066	0.020	0.043	0.057	0.035	0.065
	R	0.07	0.65	-0.75	0.59	-0.67	-0.02	0.09
2016-	Slope	0.30	0.34	0.26	0.25	0.34	0.30	0.15
	Uncertainty of slope	0.016	0.024	0.023	0.024	0.027	0.024	0.022
	R	0.99***	0.98***	0.98***	0.97***	0.99***	0.98***	0.98*

Note: *, **, *** denote $P<0.05$, $P<0.01$, $P<0.001$ respectively.

In response to the Paris Agreement's requirement of a global stocktake every five years (https://unfccc.int/sites/default/files/paris_agreement_english_.pdf), we analyze China's emissions variation every five years (Fig. 2), using 2002 as the baseline year. The highest growth is recorded in the period from 2002 to 2007 (> 0.57 Gt year^{-1}) and 2007-2012 (> 0.51 Gt year^{-1}), followed by a stable period in the years from 2012 to 2017, in which the CEADs even records a slight decline (-0.01 Gt year^{-1}). Growth then resumed in 2017-2022 and 2022-2023, averaging 0.20 Gt year^{-1} and 0.24 Gt year^{-1}, respectively.

https://doi.org/10.5194/egusphere-2025-3914
Preprint. Discussion started: 2 September 2025

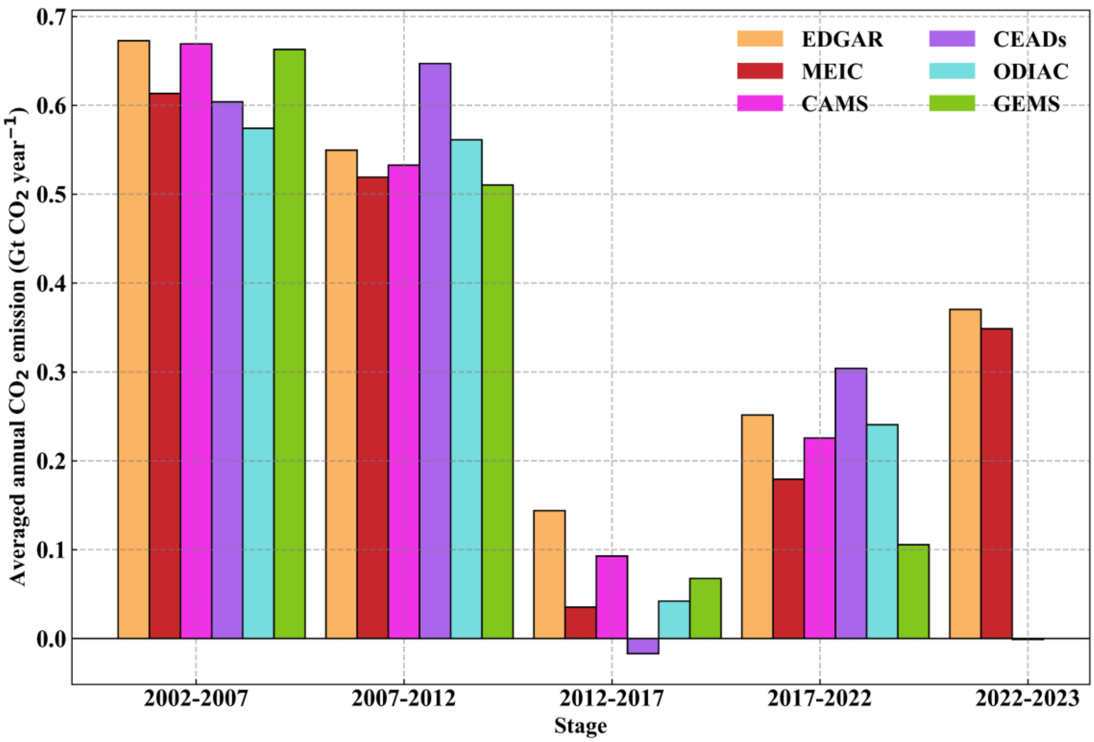

Figure 2. Average annual CO_2 emission growth rate during the five-year periods.

We use four major emission sectors defined by MEIC: electricity and heat production, industry and construction, residential and commercial, and transport (Table S1). To ensure comparability, we reclassify the sectoral CO_2 emissions in the other inventories according to this framework (Table S2). The sectoral CO_2 emissions show that the electricity and heat production sector and the industry and construction sector dominate emissions and together account for over 78% of total emissions (Fig. 3). Prior to 2016, emissions from the industry and construction exceeded emissions from the electricity and heat production. However, since 2012, the sector of industry and construction has become stable and even declined in some inventories (MEIC, CEADs, and GEMS), while the sector of electricity and heat production shows a steady upward trend after 2017. As a result, the electricity and heat production became the largest emitting sector in most inventories after 2017 (CEADs: 2016, MEIC and GEMS: 2017, EDGAR: 2018). In addition, residential and commercial emissions as well as the transport sector, show similar trends in most inventories (except GEMS). In most inventories (e.g., EDGAR, MEIC, CAMS, and CEADs), emissions from the residential and commercial sector gradually exceeded those from the transport sector after 2016, while a reverse pattern was observed in GEMS. The changes in the size of sectoral CO_2 emissions indicate the changes in China's energy structure and economic growth.

https://doi.org/10.5194/egusphere-2025-3914
Preprint. Discussion started: 2 September 2025

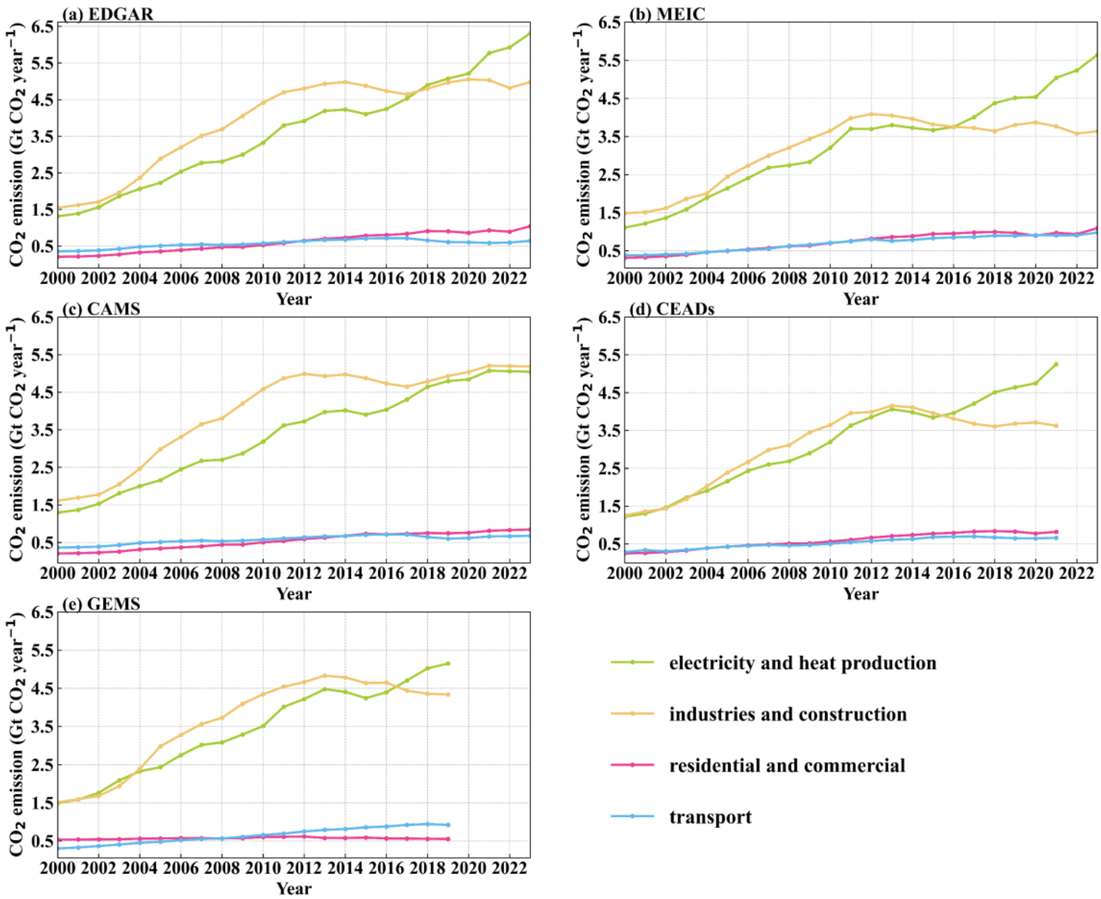

Figure 3. Anthropogenic CO_2 emissions by sector—electricity and heat production, industries and construction, residential and commercial, and transport—for the period 2000–2023, as reported by EDGAR (a), MEIC (b), CAMS (c), CEADs (d), and GEMS (e). Although CEADs provides both national- and provincial-level sectoral data, the national-level version is used here for consistency with other inventories. ODIAC does not provide sectoral CO_2 emissions.

3.2 Spatial distribution at national scale

3.2.1 Total CO_2 emissions

Since all five inventories (ODIAC, EDGAR, MEIC, CAMS, and GEMS) contain spatially explicit emission estimates for 2019, which is the latest year covered in GEMS version used in this study, we chose 2019 as the reference year for comparing the spatial patterns (Fig. 4) and the differences between the inventories using MEIC as a baseline (Fig. 5). As expected, the highest emissions are concentrated in Eastern China—especially in the North China Plain (NCP), the Beijing-Tianjin-Hebei (BTH), the Yangtze River Delta (YRD) and the Pearl River Delta (PRD)—as hotspots of anthropogenic CO_2 emissions due to high population density and industrial activity (Fig. 4a-e). ODIAC shows the most intense emissions in the eastern regions, but has large spatial gaps in the west, as it relies on nighttime lighting that does not capture emissions in poorly lit areas (Fig. 4a). This approach tends to over-allocate emissions to brightly lit urban areas, while regions with limited nighttime lighting, including

https://doi.org/10.5194/egusphere-2025-3914
Preprint. Discussion started: 2 September 2025

both sparsely populated areas and areas with high population but limited lighting, such as Western Sichuan, Inner Mongolia, and Xinjiang, are not captured.

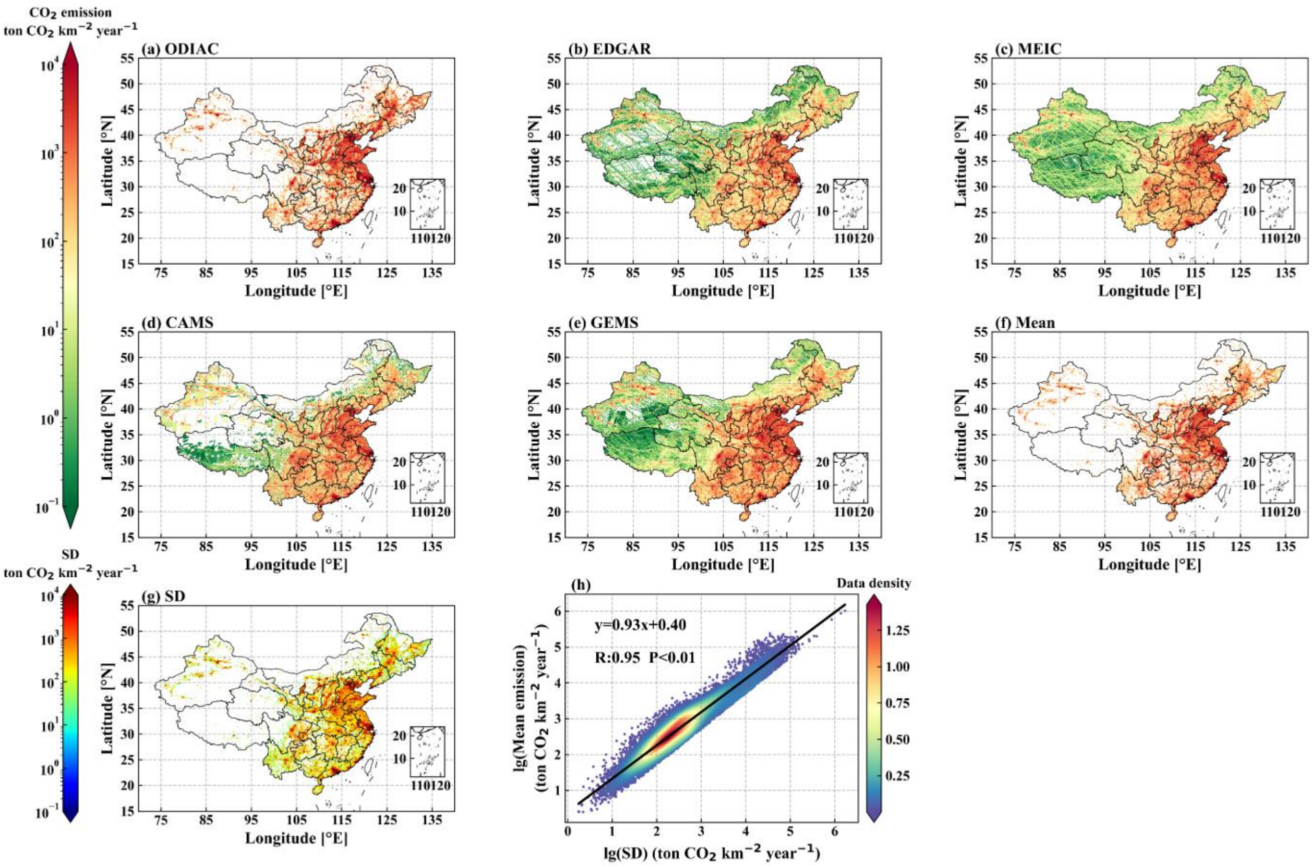

Figure 4. Spatial distribution of CO_2 emissions in 2019 at a resolution of 0.1° from ODIAC (a), EDGAR (b), MEIC (c), CAMS (d), and GEMS (e), together with the mean (f) and standard deviation (SD) (g) of the emission inventories. Sub-graph (h) shows the scatter plot illustrating the correlation between the grid-level mean emissions and the standard deviation.

https://doi.org/10.5194/egusphere-2025-3914
Preprint. Discussion started: 2 September 2025

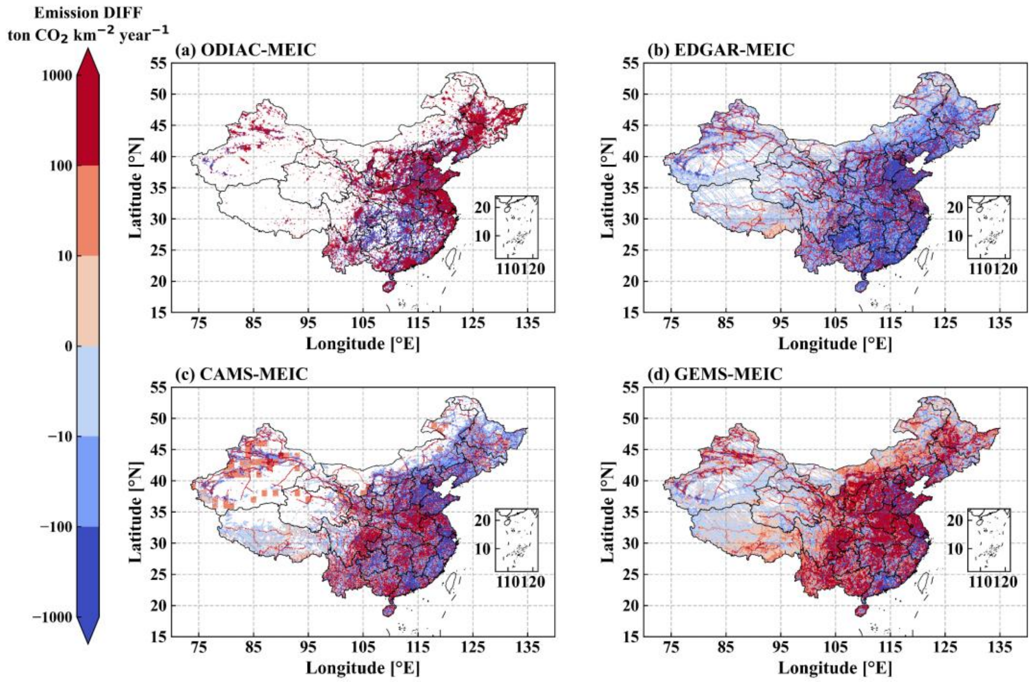

Figure 5. Spatial distribution of CO_2 emission differences in 2019 between MEIC and each of the other inventories: (a) ODIAC minus MEIC, (b) EDGAR minus MEIC, (c) CAMS minus MEIC, and (d) GEMS minus MEIC.

The SD between the five inventories (Fig. 4g) is strongly correlated with the mean of the emissions (Fig. 4f), with a slope of 0.93 and a correlation coefficient (R) of 0.95 between log-transformed estimates (Fig. 4h). This indicates that emission uncertainties are highly correlated with emission levels, and that higher uncertainties coincide with higher emissions in economic and industrial regions such as NCP, BTH, YRD, and PRD.

To assess spatial consistency, we compared ODIAC, EDGAR, CAMS, and GEMS with MEIC as a benchmark (Fig. 5). Compared to MEIC, ODIAC allocates more emissions in most coastal areas and northeastern provinces (e.g., Shandong, YRD, BTH, PRD, and Northeast China), but distributes lower CO_2 emissions in the southwest region (e.g., Guizhou, Chongqing), where population density is relatively high but satellite nightlight signals are weak (Fig. 5a). CAMS shows an opposite pattern, reporting lower emissions in most coastal and northeastern areas, but slightly higher values in parts of Jiangsu and Guangdong (Fig. 5c). GEMS shows slightly lower emissions in remote western areas (e.g., Xinjiang, Tibet, western Inner Mongolia) and relatively higher values in eastern provinces (Fig. 5d).

In space, EDGAR shows widespread lower emissions compared to MEIC, with negative differences dominating the spatial pattern (Fig. 5b). Positive differences, which are mainly concentrated along road distribution, are much rarer (only 39% of the number of negative difference grids). Despite this pattern, EDGAR yields a higher average grid-cell difference from MEIC (110.60 ton CO_2 km^{-2} $year^{-1}$) than GEMS (43.12 ton CO_2 km^{-2} $year^{-1}$), and is only moderately lower than ODIAC (171.22 ton CO_2 km^{-2} $year^{-1}$) and CAMS (168.80 ton CO_2 km^{-2} $year^{-1}$). This suggests that although the positive differences between

https://doi.org/10.5194/egusphere-2025-3914
Preprint. Discussion started: 2 September 2025

EDGAR and MEIC are spatially limited, they might be large in magnitude, potentially linking to emission hotspots such as highways or industrial clusters. We explore this further in Section 3.2.2.

3.2.2 Sectoral CO_2 emissions in EDGAR

To explain the higher average grid-cell emissions of EDGAR (110.60 ton CO_2 km^{-2} year^{-1} higher than MEIC in 2019) despite predominantly negative spatial differences, we analyze the discrepancies at the grid level (Fig. 6a). The cumulative sum of positive emission differences exceeds that of the negative ones when the absolute differences exceed 10^5 ton CO_2 km^{-2} year^{-1}. Although these extremes accounted for only 0.14% of the total grids, their cumulative magnitude (1.97×10^8 ton CO_2 km^{-2} year^{-1}) is 1.91 times the absolute sum of all remaining grids ($\leq 10^5$ ton CO_2 km^{-2} year^{-1}, totaling -1.03×10^8 ton CO_2 km^{-2} year^{-1}). This confirms that the positive average grid-cell difference of EDGAR is caused by a small number of grids with extremely high emissions ($>10^5$ ton CO_2 km^{-2} year^{-1}).

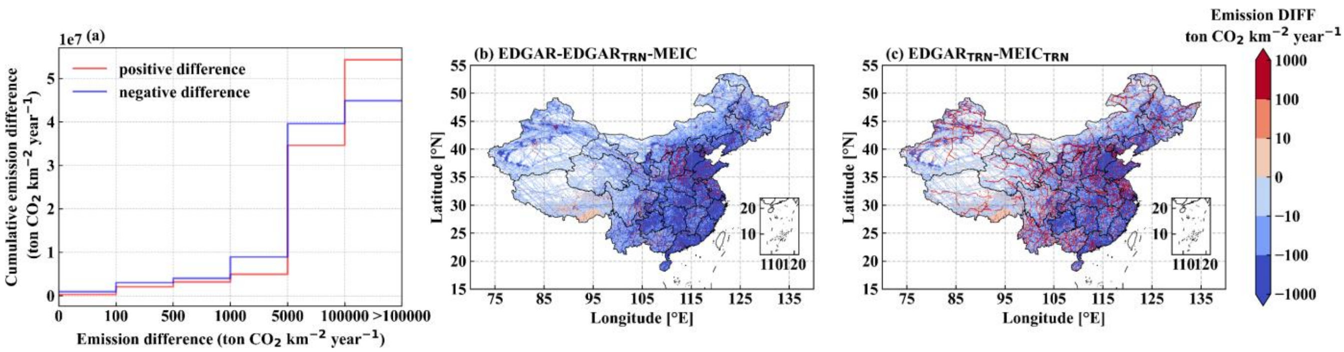

Figure 6. (a) Cumulative distribution of gridded emission differences (ton CO_2 km-2 year-1) between EDGAR and MEIC inventories. The cumulative sum for negative differences (blue line) is calculated using their absolute magnitudes and plotted against the corresponding positive values on the x-axis (i.e., 100 represents -100). The spatial distributions of the differences are shown in (b) EDGAR emissions without transport minus MEIC total emissions and (c) EDGAR transport emissions minus MEIC transport emissions.

Spatially, most of the grids with positive emission differences are shown along major road networks (Fig. 5b). When the EDGAR's transport sector is removed (Fig. 6b), the proportion of positive grids reduces drastically from 28.55% to 9.40%, confirming that the EDGAR's road transport emissions produce spatially extensive positive differences. However, the number of extreme positive emission differences ($>10^5$ ton CO_2 km^{-2} year^{-1}) remains unchanged after removing transport, suggesting that these extreme differences originate from non-transport sectors. A sectoral breakdown confirms that industry and construction contribute the most to the overall differences (1.16 Gt year^{-1}), followed by electricity and heat production (0.56 Gt year^{-1}), while residential and commercial (–0.28 Gt year^{-1}), and transport (–0.06 Gt year^{-1}) play a smaller role. Given these magnitudes, we conclude that the extremely high emitters—though few in number—are most likely from localized industrial and power generation activities, where EDGAR may allocate emissions more aggressively to point sources than MEIC. This divergence may stem from EDGAR's use of the CARMA power plant database, while MEIC uses CPED. Although CARMA

https://doi.org/10.5194/egusphere-2025-3914
Preprint. Discussion started: 2 September 2025

and CPED report similar total emissions (2% difference), CPED contains approximately 1300 more small power plants (F. Liu et al., 2015; Han et al., 2020a). CARMA's sparser coverage concentrates emissions at fewer locations, thus producing EDGAR's extreme positive grid anomalies.

Despite the small total transport discrepancy (< 0.06 Gt year^{-1}) between EDGAR and MEIC, their spatial patterns differ significantly (Fig. 6c). EDGAR concentrates transport emissions along major road networks, while MEIC distributes them more diffusely across China, which links to the different spatial allocation methods of EDGAR and MEIC. Notably, including transport emissions reduces the proportion of positive emission differences from 46.38% (non-transport only) to 28.55% (total difference). This indicates that the transport sectors of EDGAR and MEIC play a key role in the spatial pattern of positive emission differences, even though their total emissions are comparable.

3.3 CO_2 emission estimates at provincial level

3.3.1 Provincial estimates in CEADs

CEADs provides two forms of CO_2 emission estimates for provinces: the "province" series (referred to as CEADs (provinces)), which provides total emissions directly for each province, and the "sectors" series (referred to as CEADs (sectors)), which compiles fuel- and sector-specific emissions before summing them to the provincial totals. However, in some provinces, particularly Shanxi, these two estimates differ significantly (Fig. 7a). In Shanxi, CEADs (provinces) exceeds CEADs (sectors) after 2008, with the discrepancy growing from 167.03 Mt year^{-1} in 2008 to 1167.73 Mt year^{-1} in 2021. In contrast, the CEADs (sectors) closely matches the other five independent inventories (ODIAC, EDGAR, MEIC, CAMS and GEMS), with its mean emissions deviating by no more than 3.84 Mt year^{-1} from the average of the five inventories.

https://doi.org/10.5194/egusphere-2025-3914
Preprint. Discussion started: 2 September 2025

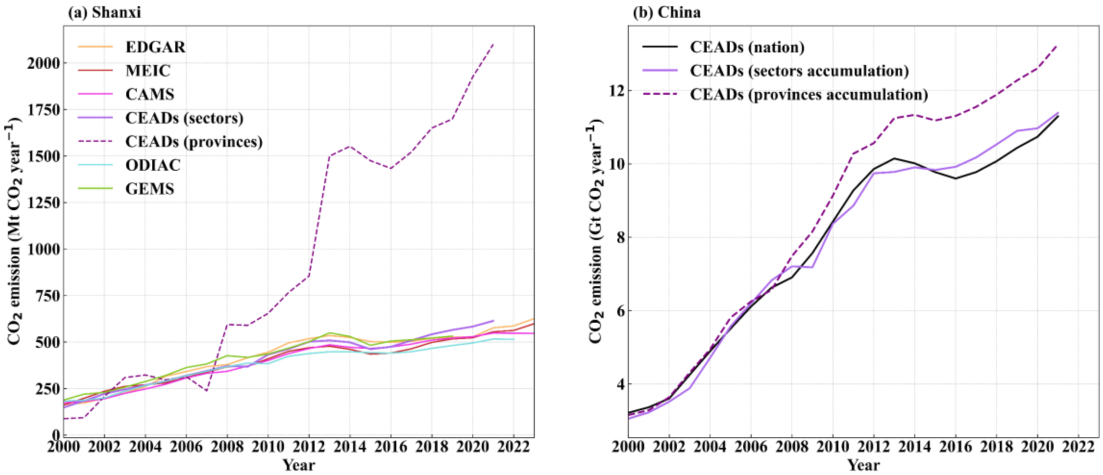

Figure 7. (a) Anthropogenic CO_2 emissions in Shanxi Province from six inventories: EDGAR, MEIC, CAMS, CEADs, ODIAC, and GEMS. CEADs provides two types of provincial-level estimates: reported provincial-level totals ("CEADs (provinces)") and aggregated sectoral emissions ("CEADs (sectors)"). Emissions from other inventories were derived by spatial aggregation of raster data. (b) Comparison between total national emissions from CEADs and the sum of provincial level emissions from CEADs (sectors) and CEADs (nation).

At the national level, we assess both provincial datasets by aggregating their values across all provinces and comparing the results with the national total reported by CEADs (Fig. 7b). When the CEADs (sectors) are summed, the reconstructed national CO_2 emissions match the national CEADs values almost perfectly, showing a mean annual deviation of only 0.01 Gt year^{-1} over the period 2000-2021. In contrast, the aggregated CEADs (provinces) reports significantly higher national totals and exceeds the national CEADs emissions by an average of 0.85 Gt year^{-1}. These comparisons demonstrate that the sector-based CEADs provides consistent provincial totals that are in line with both the independent inventories and the national compilation of CEADs. We therefore recommend using the CEADs (sectors) for all analyses at the national and provincial levels.

3.3.2 Comparison of emission inventories in typical provinces

The mean and SD of the provincial CO_2 emissions from 2000 to 2023 are shown in Figure S1. To investigate the causes of the discrepancies in the inventories, we select a subset of representative provinces for a detailed comparison. Representative provinces are identified using the SD and the mean emissions between the six emission inventories, calculated for the period 2000-2023. Each year, all provinces are ranked based on these two metrics, and cumulative scores are calculated by summing the annual ranks over the entire 24-year period (2000-2023). The top six provinces in each category are selected, resulting in a list of nine representative provinces (some provinces repeat in the ranking of the two metrics): Inner Mongolia, Liaoning, Hebei, Shandong, Henan, Hubei, Shanghai, Jiangsu, and Guangdong (Table 3). In the third emissions phase (2016–2023), each of the six provinces with the highest emissions contributes more than 5.4 % of total national emissions, and together they account for almost 40 % of China's emissions. To investigate the emission patterns and cross-inventory agreement, we examine the CO_2 emissions of these nine representative provinces (Fig. 8).

https://doi.org/10.5194/egusphere-2025-3914
Preprint. Discussion started: 2 September 2025

Table 3. The top six provincial-level regions with the highest cumulative CO_2 emissions and the highest SD among the inventories (2000–2023), and CO_2 emission percentage of the top six provinces with the highest emissions from 2016 to 2023.

Top six provinces by mean emissions	Cumulative rank score	CO_2 emission fractions (2016-2023)	Top six provinces by SD	Cumulative rank score
Shandong	24	8.43%	Hubei	67
Jiangsu	53	7.48%	Hebei	69
Hebei	72	6.37%	Guangdong	106
Guangdong	112	5.71%	Liaoning	114
Henan	115	5.41%	Shandong	120
Inner Mongolia	148	6.15%	Shanghai	136

Note: Cumulative rank score refers to the sum of a province's annual rank (from highest to lowest) in terms of mean emissions or inter-inventory standard deviation (SD)

https://doi.org/10.5194/egusphere-2025-3914
Preprint. Discussion started: 2 September 2025

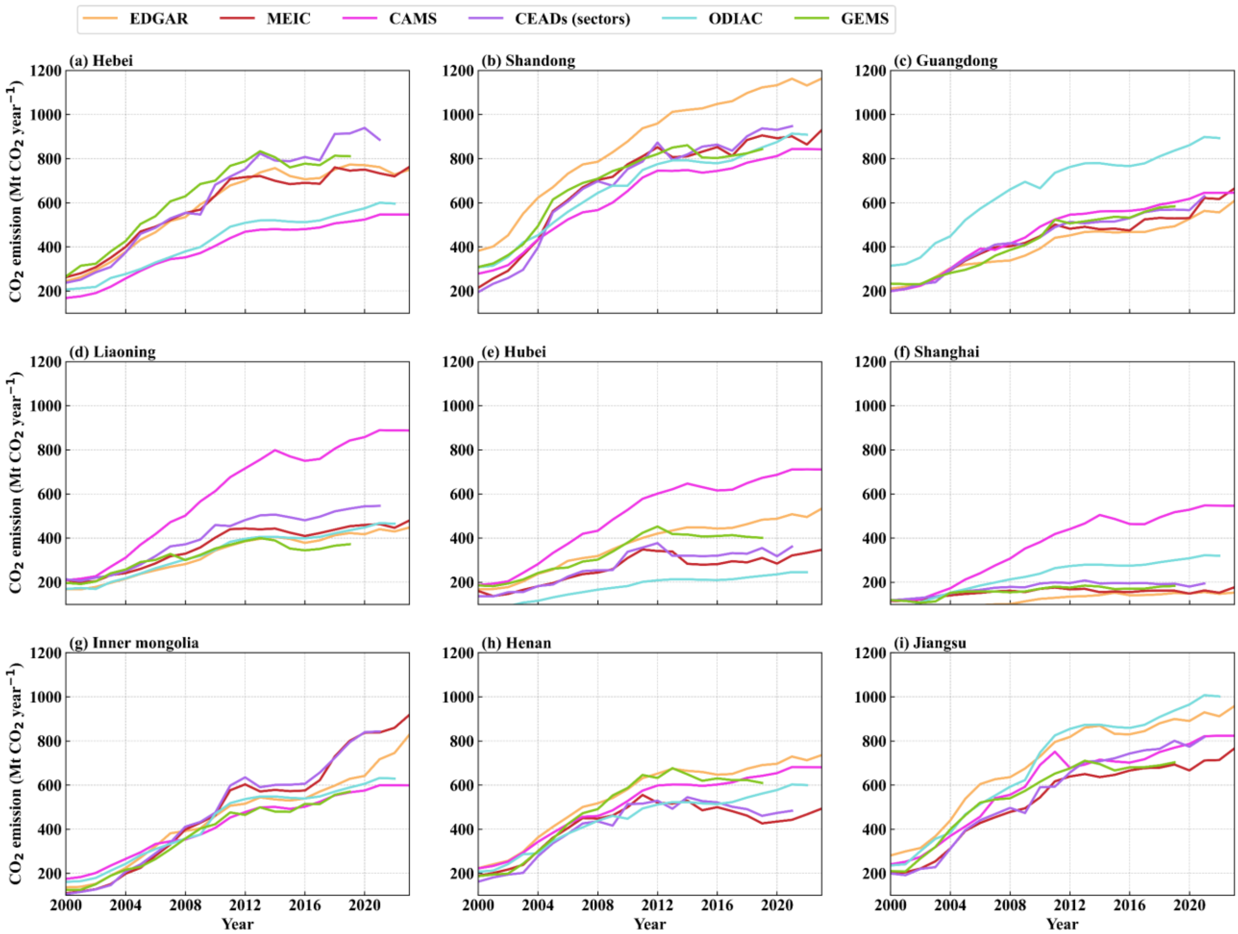

Figure 8. Anthropogenic CO_2 emissions from 2000 to 2023 for nine typical provinces: Hebei (a), Shandong (b), Guangdong (c), Liaoning (d), Hubei (e), Shanghai (f), Inner Mongolia (g), Henan (h), and Jiangsu (i). These provinces are selected based on either the highest average emissions or the highest SD among the inventories.

Among the provinces with higher emissions, Hebei, Shandong, and Guangdong rank at the top in terms of both mean emissions and SD (Table 3). In Hebei (Fig. 8a), CAMS and ODIAC report emissions averaging 416 Mt year^{-1}, which is 32% less than the other four inventories (618 Mt year^{-1}), thereby contributing significantly to the SD. In Shandong (Fig. 8b), all inventories show increased emissions, but EDGAR (873 Mt year^{-1} on average) reports emissions over 30% higher than the others (670 Mt year^{-1}), resulting in a pronounced dispersion. Guangdong (Fig. 8c) shows a pronounced ODIAC bias, with an average of 663 Mt year^{-1}, over 53% higher than the average of the other five inventories (433 Mt year^{-1}). It is noteworthy that ODIAC significantly distributes more emissions in Jiangsu, Shanghai and Guangdong—especially in the latter two provinces. This suggests that the downscaling approach in ODIAC may overweight emissions in dense urban agglomeration (or city cluster).

Liaoning, Hubei, and Shanghai (Fig. 8d-f) are selected due to their larger inter-inventory SD. In these provinces, CAMS exceeds the mean of the five inventories by 50-90% in Liaoning, 60-110% in Hubei, and 50-230% in Shanghai, which increases the dispersion. In Hubei, the high SD is also due to persistent dispersion across all six inventories (Fig. 8e). CAMS consistently provides the highest estimates, while ODIAC provides the lowest, making Hubei the province with the highest SD, despite average CO_2 emissions being only moderate.

Inner Mongolia, Henan, and Jiangsu (Fig. 8g-i) are selected for their high emissions rather than their extreme dispersion. Inner Mongolia followed the national three-stage growth pattern, with MEIC and CEADs—both China-tailored inventories—matching within 11 Mt year^{-1} and even outperforming other inventories after 2016 (Fig. 8g). In Henan, domestic inventories (MEIC and CEADs) show two distinct phases: growth until 2012, followed by a decline, while the other global-based inventories (except GEMS) slowly increase after 2016 (Fig. 8h). In Jiangsu, all inventories show a two-phase trend, with rapid growth before 2012 and relative stabilization thereafter. After 2012, ODIAC and EDGAR report the highest emissions in Jiangsu, while MEIC shows the lowest trend (Fig. 8j). In the nine provinces, CEADs and MEIC estimates are largely consistent, especially in Inner Mongolia, Shandong, Henan, Hubei, and Shanghai.

Comparing the variability of emissions in the nine provinces and at the national level, the coefficient of variation (CV = SD/mean; Fig. S2) for total national emissions in China is the lowest and most stable for the period 2000-2023. In contrast, the time-averaged CV of the nine provinces with high emissions is at least 2.8 times higher than the national average (0.044). Liaoning, Hubei, and Shanghai, which show the largest SD between inventories, have even higher CVs, with values of 0.45, 0.34, and 0.26, respectively. These values exceed the national CV by a factor of 5, while Shanghai's CV exceeds the national CV by a factor of 10. This contrast emphasizes that the uncertainties at the provincial level (10-50%) are larger than the deviations at the national level (<5%), which is due to systematic biases in certain inventories and their different downscaling methods. We suggest establishing more ground-based CO_2 monitoring sites to verify and estimate anthropogenic CO_2 emissions in these provinces.

4 Conclusions and discussion

China's annual anthropogenic CO_2 total emission increases from 3.42 Gt in 2000 to 12.03 Gt in 2023. The discrepancies among the inventories have widened from 0.41 Gt year^{-1} to 1.63 Gt year^{-1}, which is mainly due to the highest estimates reported from EDGAR and the lowest values estimated from MEIC, especially after 2012. Our results are consistent with L. Zheng et al. (2025) but opposite to Han et al. (2020a), demonstrating the differences in emission versions (Our study: EDGAR2024, MEIC-global-CO_2 v1.0; Zheng: EDGAR v7.0, MEIC-China-CO_2 v1.4; Han: EDGAR v4.3.2, MEIC-China-CO_2 v1.3).

The six inventories in this study agree on three emission phases: a rapid increase of 0.56 ± 0.015 Gt year^{-1} (2000–2012), a near-stagnation phase of 0.01 ± 0.045 Gt year^{-1} under the 12th Five-Year Plan (2012–2016), and a renewed growth of 0.30 ± 0.016 Gt year^{-1} (2016–2023), with recent increases highlighting the challenges in controlling anthropogenic CO_2 emissions. In terms of emission sectors, emissions are dominated by electricity and heat production, industry and construction (together accounting for 78% of total emissions). The former source overtook the latter as the largest source after 2017, reflecting changes in China's energy structure.

https://doi.org/10.5194/egusphere-2025-3914
Preprint. Discussion started: 2 September 2025

In spatial terms, the higher emissions strongly corresponded with the higher uncertainty (reference 2019: R = 0.95, P< 0.01). Eastern regions, particularly the BTH, YRD, and PRD city clusters, had both the highest emissions and the largest SD. This pattern confirms the finding of Wang et al. (2013) that areas with high emission level have the largest uncertainties. Different allocation methods are the main reason for the spatial discrepancies between the inventories. The ODIAC nightlight proxy distributes more emissions in urban areas and fewer emissions in the western regions. EDGAR, which is based on the CARMA database, concentrated power plant emissions on fewer grids, resulting in extreme anomalies where the difference (EDGAR-MEIC) exceeds 10^5 ton CO_2 km^{-2} $year^{-1}$. In contrast, MEIC uses the more detailed CPED and distributes similar total CO_2 emissions (difference within 2% of CARMA) across a larger number of power plants (Liu et al., 2015). The overall spatial grid-based difference between EDGAR and MEIC is dominated by negative values (71.45% of grids), due to the different allocation methods for the transport sector. EDGAR allocates emissions along major roads, while MEIC uses a more diffuse distribution. Despite a minimal overall difference in the sector of transport (< 0.06 Gt), the spatial mismatch was substantial, with 70.37% of transport-related grid differences being negative, due to the different disaggregation methods: OpenStreetMap and OpenRailwayMap in EDGAR versus CDRM in MEIC.

At the provincial level, CEADs data show critical inconsistencies: its provincial sectoral emissions are consistent with the multi-inventory means, but the provincial series reports lower emissions in Shanxi by more than 127% (approximately 500 Mt $year^{-1}$). We therefore recommend sector-based CEADs for province-level analyses. The uncertainty in the province scale is significantly higher than the national scale. For example, the coefficient of variation (CV) of Shanghai (0.45) is ten times higher than the national CV (0.044). The pronouncedly higher emissions in the coastal megacities (e.g., Shanghai, Jiangsu, and Guangdong) by ODIAC and the abnormal increase in CAMS by 50-230% in Liaoning, Hubei, and Shanghai exacerbate this divergence. Overall, reliable emissions quantification requires scale-appropriate inventories (e.g., the sectoral CEADs emissions versus the province-based CEADs emissions), improved spatial proxies (e.g., CPED vs. CARMA), and ensemble approaches to mitigate biases, especially in the carbon-intensive eastern regions.

Data availability

The emission inventories datasets are publicly available: ODIAC (https://db.cger.nies.go.jp/dataset/ODIAC/DL_odiac2023.html), EDGAR (https://edgar.jrc.ec.europa.eu/dataset_ghg2024), MEC (http://meicmodel.org.cn/?page_id=2341), CAMS (https://eccad.sedoo.fr/#/metadata/479), GEMS (https://gems.pku.edu.cn/home) and CEADs (https://www.ceads.net.cn/).

Author contribution

HY, KW, and MZ designed the study. HY evaluated the data and wrote the paper with the help of KW and MZ. HS and GJ-M provided valuable suggestions to improve the manuscript. All authors read and provided comments on the paper.

Competing interests

The authors declare that they have no conflict of interest.

Acknowledgements

This study is supported by the National Key Research and Development Program of China (No. 2023YFB3907500, 2023YFB3907505) and the Basic Research Project of the Institute of Atmospheric Physics, Chinese Academy of Sciences (E468131801). We gratefully acknowledge the data providers of the emission inventories used in this study: the ODIAC dataset developed by the Global Carbon Project Center for Global Environmental Research (CGER) at the National Institute for Environmental Studies (NIES), Japan, led by Dr. Tomohiro Oda; the EDGAR dataset maintained and publicly released by the Joint Research Centre (JRC) of the European Commission; the MEIC inventory developed by Tsinghua University under the direction of Dr. Qiang Zhang; the CAMS inventory jointly developed by the Copernicus Atmosphere Monitoring Service (CAMS) at the European Centre for Medium-Range Weather Forecasts (ECMWF) on behalf of the European Commission, with contributions from Dr. Antonin Soulie; the GEMS inventory developed by a joint team from Peking University and Southern University of Science and Technology; and the CEADs inventory, also developed by Tsinghua University, with contributions from Dr. Dabo Guan.

References

Akimoto, H., Ohara, T., Kurokawa, J., and Horii, N.: Verification of energy consumption in China during 1996–2003 by using satellite observational data, Atmospheric Environment, 40, 7663–7667, https://doi.org/10.1016/j.atmosenv.2006.07.052, 2006.

Andres, R. J., Boden, T. A., and Higdon, D. M.: Gridded uncertainty in fossil fuel carbon dioxide emission maps, a CDIAC example, Atmospheric Chemistry and Physics, 16, 14979–14995, https://doi.org/10.5194/acp-16-14979-2016, 2016.

Cai, B., Liang, S., Zhou, J., Wang, J., Cao, L., Qu, S., Xu, M., and Yang, Z.: China high resolution emission database (CHRED) with point emission sources, gridded emission data, and supplementary socioeconomic data, Resources, Conservation and Recycling, 129, 232–239, https://doi.org/10.1016/j.resconrec.2017.10.036, 2018.

Etheridge, D. M., Steele, L. P., Langenfelds, R. L., Francey, R. J., Barnola, J.-M., and Morgan, V. I.: Natural and anthropogenic changes in atmospheric CO_2 over the last 1000 years from air in Antarctic ice and firn, Journal of Geophysical Research: Atmospheres, 101, 4115–4128, https://doi.org/10.1029/95JD03410, 1996.

Guan, D., Liu, Z., Geng, Y., Lindner, S., and Klaus, H.: The gigatonne gap in China's carbon dioxide inventories, Nature Climate Change, 2, 672–675, https://doi.org/10.1038/nclimate1560, 2012.

Guan, Y., Shan, Y., Huang, Q., Chen, H., Wang, D., and Hubacek, K.: Assessment to China's Recent Emission Pattern Shifts, Earth's Future, 9, e2021EF002241, https://doi.org/10.1029/2021EF002241, 2021a.

Guan, Y., Shan, Y., Huang, Q., Chen, H., Wang, D., and Hubacek, K.: Assessment to China's Recent Emission Pattern Shifts, Earth's Future, 9, e2021EF002241, https://doi.org/10.1029/2021EF002241, 2021b.

Han, P., Zeng, N., Oda, T., Zhang, W., Lin, X., Liu, D., Cai, Q., Ma, X., Meng, W., Wang, G., Wang, R., and Zheng, B.: A city-level comparison of fossil-fuel and industry processes-induced CO_2 emissions over the Beijing-Tianjin-Hebei region from eight emission inventories, Carbon Balance Manage, 15, 25, https://doi.org/10.1186/s13021-020-00163-2, 2020a.

Han, P., Zeng, N., Oda, T., Lin, X., Crippa, M., Guan, D., Janssens-Maenhout, G., Ma, X., Liu, Z., Shan, Y., Tao, S., Wang, H., Wang, R., Wu, L., Yun, X., Zhang, Q., Zhao, F., and Zheng, B.: Evaluating China's fossil-fuel CO_2 emissions from a comprehensive dataset of nine inventories, Atmospheric Chemistry and Physics, 20, 11371–11385, https://doi.org/10.5194/acp-20-11371-2020, 2020b.

Hong, C., Zhang, Q., He, K., Guan, D., Li, M., Liu, F., and Zheng, B.: Variations of China's emission estimates: response to uncertainties in energy statistics, Atmospheric Chemistry and Physics, 17, 1227–1239, https://doi.org/10.5194/acp-17-1227-2017, 2017.

Janssens-Maenhout, G., Crippa, M., Guizzardi, D., Muntean, M., Schaaf, E., Dentener, F., Bergamaschi, P., Pagliari, V., Olivier, J. G. J., Peters, J. A. H. W., van Aardenne, J. A., Monni, S., Doering, U., Petrescu, A. M. R., Solazzo, E., and Oreggioni, G. D.: EDGAR v4.3.2 Global Atlas of the three major greenhouse gas emissions for the period 1970–2012, Earth System Science Data, 11, 959–1002, https://doi.org/10.5194/essd-11-959-2019, 2019.

Li, M., Liu, H., Geng, G., Hong, C., Liu, F., Song, Y., Tong, D., Zheng, B., Cui, H., Man, H., Zhang, Q., and He, K.: Anthropogenic emission inventories in China: a review, National Science Review, 4, 834–866, https://doi.org/10.1093/nsr/nwx150, 2017a.

Li, M., Zhang, Q., Kurokawa, J., Woo, J.-H., He, K., Lu, Z., Ohara, T., Song, Y., Streets, D. G., Carmichael, G. R., Cheng, Y., Hong, C., Huo, H., Jiang, X., Kang, S., Liu, F., Su, H., and Zheng, B.: MIX: a mosaic Asian anthropogenic emission inventory under the international collaboration framework of the MICS-Asia and HTAP, Atmos. Chem. Phys., 17, 935–963, https://doi.org/10.5194/acp-17-935-2017, 2017b.

Liu, F., Zhang, Q., Tong, D., Zheng, B., Li, M., Huo, H., and He, K. B.: High-resolution inventory of technologies, activities, and emissions of coal-fired power plants in China from 1990 to 2010, Atmospheric Chemistry and Physics, 15, 13299–13317, https://doi.org/10.5194/acp-15-13299-2015, 2015.

Liu, H., Hu, C., Xiao, Q., Zhang, J., Sun, F., Shi, X., Chen, X., Yang, Y., and Xiao, W.: Analysis of anthropogenic CO_2 emission uncertainty and influencing factors at city scale in Yangtze River Delta region: One of the world's largest emission hotspots, Atmospheric Pollution Research, 15, 102281, https://doi.org/10.1016/j.apr.2024.102281, 2024.

Oda, T. and Maksyutov, S.: A very high-resolution (1 km×1 km) global fossil fuel CO_2 emission inventory derived using a point source database and satellite observations of nighttime lights, Atmospheric Chemistry and Physics, 11, 543–556, https://doi.org/10.5194/acp-11-543-2011, 2011.

Oda, T., Maksyutov, S., and Andres, R. J.: The Open-source Data Inventory for Anthropogenic CO_2, version 2016 (ODIAC2016): a global monthly fossil fuel CO_2 gridded emissions data product for tracer transport simulations and surface flux inversions, Earth System Science Data, 10, 87–107, https://doi.org/10.5194/essd-10-87-2018, 2018.

Oda, T., Bun, R., Kinakh, V., Topylko, P., Halushchak, M., Marland, G., Lauvaux, T., Jonas, M., Maksyutov, S., Nahorski, Z., Lesiv, M., Danylo, O., and Horabik-Pyzel, J.: Errors and uncertainties in a gridded carbon dioxide emissions inventory, Mitig Adapt Strateg Glob Change, 24, 1007–1050, https://doi.org/10.1007/s11027-019-09877-2, 2019.

Peylin, P., Law, R. M., Gurney, K. R., Chevallier, F., Jacobson, A. R., Maki, T., Niwa, Y., Patra, P. K., Peters, W., Rayner, P. J., Rödenbeck, C., van der Laan-Luijkx, I. T., and Zhang, X.: Global atmospheric carbon budget: results from an ensemble of atmospheric CO_2 inversions, Biogeosciences, 10, 6699–6720, https://doi.org/10.5194/bg-10-6699-2013, 2013.

https://doi.org/10.5194/egusphere-2025-3914
Preprint. Discussion started: 2 September 2025

Schleussner, C.-F., Rogelj, J., Schaeffer, M., Lissner, T., Licker, R., Fischer, E. M., Knutti, R., Levermann, A., Frieler, K., and Hare, W.: Science and policy characteristics of the Paris Agreement temperature goal, Nature Clim Change, 6, 827–835, https://doi.org/10.1038/nclimate3096, 2016.

Shan, Y., Guan, D., Zheng, H., Ou, J., Li, Y., Meng, J., Mi, Z., Liu, Z., and Zhang, Q.: China CO_2 emission accounts 1997–2015, Sci Data, 5, 170201, https://doi.org/10.1038/sdata.2017.201, 2018.

Shan, Y., Huang, Q., Guan, D., and Hubacek, K.: China CO_2 emission accounts 2016–2017, Sci Data, 7, 54, https://doi.org/10.1038/s41597-020-0393-y, 2020.

Soulie, A., Granier, C., Darras, S., Zilbermann, N., Doumbia, T., Guevara, M., Jalkanen, J.-P., Keita, S., Liousse, C., Crippa, M., Guizzardi, D., Hoesly, R., and Smith, S. J.: Global anthropogenic emissions (CAMS-GLOB-ANT) for the Copernicus Atmosphere Monitoring Service simulations of air quality forecasts and reanalyses, Earth Syst. Sci. Data, 16, 2261–2279, https://doi.org/10.5194/essd-16-2261-2024, 2024.

Wang, R., Tao, S., Ciais, P., Shen, H. Z., Huang, Y., Chen, H., Shen, G. F., Wang, B., Li, W., Zhang, Y. Y., Lu, Y., Zhu, D., Chen, Y. C., Liu, X. P., Wang, W. T., Wang, X. L., Liu, W. X., Li, B. G., and Piao, S. L.: High-resolution mapping of combustion processes and implications for CO₂ emissions, Atmos. Chem. Phys., 13, 5189–5203, https://doi.org/10.5194/acp-13-5189-2013, 2013.

Xia, L., Liu, R., Fan, W., and Ren, C.: Emerging carbon dioxide hotspots in East Asia identified by a top-down inventory, Commun Earth Environ, 6, 1–13, https://doi.org/10.1038/s43247-024-01991-7, 2025.

Xu, J., Guan, Y., Oldfield, J., Guan, D., and Shan, Y.: China carbon emission accounts 2020-2021, Applied Energy, 360, 122837, https://doi.org/10.1016/j.apenergy.2024.122837, 2024a.

Xu, R., Tong, D., Xiao, Q., Qin, X., Chen, C., Yan, L., Cheng, J., Cui, C., Hu, H., Liu, W., Yan, X., Wang, H., Liu, X., Geng, G., Lei, Y., Guan, D., He, K., and Zhang, Q.: MEIC-global-CO_2: A new global CO_2 emission inventory with highly-resolved source category and sub-country information, Sci. China Earth Sci., 67, 450–465, https://doi.org/10.1007/s11430-023-1230-3, 2024b.

Zhao, Y., Nielsen, C. P., and McElroy, M. B.: China's CO_2 emissions estimated from the bottom up: Recent trends, spatial distributions, and quantification of uncertainties, Atmospheric Environment, 59, 214–223, https://doi.org/10.1016/j.atmosenv.2012.05.027, 2012.

Zheng, B., Tong, D., Li, M., Liu, F., Hong, C., Geng, G., Li, H., Li, X., Peng, L., Qi, J., Yan, L., Zhang, Y., Zhao, H., Zheng, Y., He, K., and Zhang, Q.: Trends in China's anthropogenic emissions since 2010 as the consequence of clean air actions, Atmospheric Chemistry and Physics, 18, 14095–14111, https://doi.org/10.5194/acp-18-14095-2018, 2018.

Zheng, L., Li, S., Hu, X., Zheng, F., Cai, K., Li, N., and Chen, Y.: Spatiotemporal comparative analysis of three carbon emission inventories in mainland China, Atmospheric Pollution Research, 16, 102417, https://doi.org/10.1016/j.apr.2025.102417, 2025.